

## Reverse Monte Carlo study of spherical sample under non-periodic boundary conditions: the structure of Ru nanoparticles based on x-ray diffraction data

This content has been downloaded from IOPscience. Please scroll down to see the full text.

2013 J. Phys.: Condens. Matter 25 454211

(<http://iopscience.iop.org/0953-8984/25/45/454211>)

View [the table of contents for this issue](#), or go to the [journal homepage](#) for more

Download details:

IP Address: 141.209.165.173

This content was downloaded on 21/10/2013 at 14:46

Please note that [terms and conditions apply](#).

# Reverse Monte Carlo study of spherical sample under non-periodic boundary conditions: the structure of Ru nanoparticles based on x-ray diffraction data

Orsolya Gereben<sup>1</sup> and Valeri Petkov<sup>2</sup>

<sup>1</sup> Institute for Solid State Physics and Optics, Wigner Research Centre for Physics, Hungarian Academy of Sciences, PO Box 49, H-1525 Budapest, Hungary

<sup>2</sup> Department of Physics, 203 Dow Science, Central Michigan University, Mt. Pleasant, MI 48859, USA

E-mail: [orsolya.gereben@ardeus.com](mailto:orsolya.gereben@ardeus.com)

Received 20 November 2012, in final form 11 March 2013

Published 18 October 2013

Online at [stacks.iop.org/JPhysCM/25/454211](http://stacks.iop.org/JPhysCM/25/454211)

## Abstract

A new method to fit experimental diffraction data with non-periodic structure models for spherical particles was implemented in the reverse Monte Carlo simulation code. The method was tested on x-ray diffraction data for ruthenium (Ru) nanoparticles approximately 5.6 nm in diameter. It was found that the atomic ordering in the ruthenium nanoparticles is quite distorted, barely resembling the hexagonal structure of bulk Ru. The average coordination number for the bulk decreased from 12 to 11.25. A similar lack of structural order has been observed with other nanoparticles (e.g. Petkov *et al* 2008 *J. Phys. Chem. C* **112** 8907–11) indicating that atomic disorder is a widespread feature of nanoparticles less than 10 nm in diameter.

(Some figures may appear in colour only in the online journal)

## 1. Introduction

With current technology moving fast into smaller dimensions, nanoparticles (NPs) are produced at an increased rate and explored for various applications [1–6]. The unique functionality of NPs is due to finite size effects which considerably modify their atomic-scale structure and, hence, properties. Also, NPs have a large surface to volume ratio and can interact with their environment, which is very beneficial for biomedical [7] and catalytic applications [8]. Since the atomic-scale structure predetermines the material's properties to a great extent, a big effort is underway to develop scientific tools for determining the atomic ordering in NPs. The task is not trivial since, contrary to the case of bulk crystals, atoms in NPs do not sit on the vertices of periodic lattices [9]. Furthermore, atoms at the surface of NPs are less constrained than those in the NPs' core and so prone to larger scale

structural fluctuations. This renders the atomic ordering in NPs essentially non-homogeneous, with a higher degree of order in the NPs' interior and a smaller degree of order at their surface.

Traditionally the atomic-scale structure of materials is obtained through diffraction-based techniques [9–11]. Combining diffraction data with reverse Monte Carlo simulations (RMC) [12, 13] has turned out to be very useful in structure studies of substantially disordered materials such as amorphous semiconductors [14], glasses [15] and liquids [16].

Being finite, i.e. essentially non-periodic, and structurally not quite homogeneous, the atomic-scale structure of NPs poses a serious problem, known as the nanostructure problem [17]. The problem has been tackled by several techniques with different amounts of success. For example, traditional transmission electron microscopy (TEM) can provide information about the NPs' size and morphology [18, 19].

Yet TEM images are a projection down an axis and so not so sensitive to the atomic ordering inside NPs, although a combination of aberration-corrected scanning transmission electron microscopy, statistical parameter estimation theory and discrete tomography resulted in a 3D reconstruction of the structure of a silver nanoparticle embedded in an aluminum matrix [20]. Extended x-ray absorption fine structure (EXAFS) is also very useful but yields information about the atomic ordering extending out to 5–6 Å only. Thus, for example, an EXAFS experiment would hardly distinguish between a hexagonal (hcp) and a face centered cubic (fcc) ordering of atoms since both show first and second coordination spheres of twelve and six atoms, respectively.

Among other techniques, total scattering experiments coupled with Fourier-transform, atomic radial distribution function (rdf), also called pair distribution function (PDF) analysis, and computer simulations are becoming more widely used in nanostructure studies [21, 22]. Depending on the degree of atomic ordering in NPs, different simulation techniques are employed to fit the experimental PDF data. When NPs show considerable atomic order, crystalline lattice-based models are employed that perform a least-square fit between model calculated and experimental PDF data [23] in a manner similar to the Rietveld refinement of powder diffraction data. When the degree of atomic ordering in NPs is low, simulated annealing [24] and reverse Monte Carlo (RMC) [12, 25] do a better job. In the latter type of modeling structural constraints imposed on atomic coordination numbers, bond angles soon turn out to be very useful for improving the simulations' convergence and the reliability of the produced structure models [26, 27]. Last but not least, the good capabilities of the Debye function approach in structure studies of NPs have to be acknowledged as well [28]. Several comprehensive reviews on the various modeling techniques applied in nanostructure studies are available [29].

A particular feature of all the modeling techniques mentioned above is that they apply periodic boundary conditions on the model NP structures which, among other things, makes the positions of atoms in NPs very strongly correlated with each other. Real NPs are, however, finite and have an open surface where the periodicity of the atomic ordering is ultimately broken. If the rdf of a spherical sample put inside a simulation box is calculated, then the rdf would curve downward with increasing distance instead of tending to one. In an attempt to take into account the finite size of NPs, correction factors have been developed to modify the computed radial distribution function [30]. Such correction factors are useful but still work under the assumption of infinite periodicity of the atomic ordering in NPs and so just circumvent and do not solve the nanostructure problem.

We undertook the task to develop a version of the RMC code, which will explicitly take into account the finite size and broken periodicity of NPs. Here we describe the approach we developed in some detail and the results of its testing on Ru particles that are approximately 28 Å in radius. The new methodology was included in the simulation package RMC\_POT [31, 32]. Note that production of Ru nanoparticles

is being attempted by various synthetic routes using different substrates such as graphene [33], glassy carbon [34], a metal–organic frame [35], an acetate/polyol-base [36] or in aqueous solution [37], and are vigorously explored for catalytic applications [36].

## 2. Methodology details

### 2.1. Derivation of a volume element for non-periodic boundary conditions

By definition the rdf,  $g(r) = \rho(r)/\rho_0$ , where  $\rho(r)$  is the average local and  $\rho_0$  the average atomic number density, oscillates about one at large  $r$  values. (Usually  $\rho(r)$  is only called the local number density, but now it has to be distinguished from the local density around one particular atom, so that is why it will be referred to as the average local number density.) To ensure that the model  $g(r)$  computed under non-periodic boundary conditions behaves in this way, the derivation of the average local density  $\rho(r)$  had to be modified.

Usually the partial average local density at distance  $r$  from an atom of type  $b$  with respect to a central atom of type  $a$  is calculated from an average partial histogram,  $\bar{n}_{ab}(r)$ . In the case of  $r < L$ , where  $L$  is half of the simulation box length, the following definition can be applied (1):

$$\bar{\rho}_{ab}(r) = \frac{\bar{n}_{ab}(r)}{\Delta V(r)} = \frac{\bar{n}_{ab}(r)}{4/3\pi(r_u^3 - r_l^3)} \quad (1)$$

$$\bar{n}_{ab}(r) = \frac{1}{N_a} \sum_{m=1}^{N_a} n_{ab}^m(r) \quad (2)$$

where  $r_u, r_l$  are the upper and lower boundaries of the histogram bin,  $r$  is the position of that bin's center,  $N_a$  is the total number of atoms of type  $a$  and  $n_{ab}^m(r)$  is the local partial histogram of the  $m$ th atom of type  $a$  for neighbors of type  $b$ . Here it is assumed that for every central atom of type  $a$  the volume of the  $i$ th histogram bin,  $\Delta V(r)$ , depends only on the distance  $r$  from the central atom, and not on the position of the central atom inside the simulation cell. This is so because, under periodic boundary conditions, the cell is surrounded with its mirror images.

From the average local density, the rdf,  $g(r)$ , can be calculated as follows:

$$g_{ab}(r) = \frac{\bar{\rho}_{ab}(r)}{\rho_b} = \frac{\bar{\rho}_{ab}(r)V}{N_b} \quad (3)$$

where  $N_b$  is the total number of atoms of type  $b$  and  $V$  is the simulation box volume.

Our model system under non-periodic boundary conditions will consist of a spherical sample placed into a cubic simulation box. It will represent a system with spherical particles with a known size, and narrow size distribution. It will only account for the intra-particle correlations, but as most of the inter-particle correlations are on a larger distance scale the corresponding scattering would only appear in the small angle scattering region, and would not affect the simulation result.

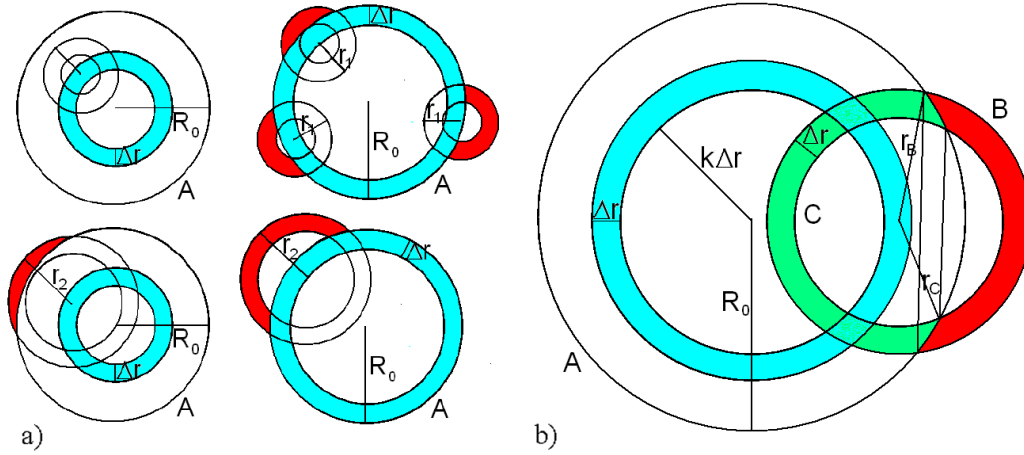


**Figure 1.** (a) Showing volume elements depending on the central atom’s position found inside the light blue zone (left side of figure: closer to the center of the sample, right side of figure: close to the surface of the sample) and the size of the histogram bin, a smaller one depicted as  $r_1$  (upper part of figure) and a larger one depicted as  $r_2$  (lower part of figure). Protruding volume elements of a histogram bin that is outside sphere A with radius  $R_0$  are shown in red. (b) The protruding part of a volume element (red) that should be subtracted from the spherical shells B and C. The volume element that is used in the normalization of the histogram is shown in green. The central atom is located on the blue ring.

In the case of non-periodic boundary conditions, the volume of the histogram bin may not be the same for the same atomic neighbor distances. Rather it will depend on  $r$  and the position of the central atom in the simulation box, that is the distance  $d$  of the central atom from the origin (see figure 1(a)). As can be seen in the figure, for some central atoms this volume element protrudes from the spherical surface of the sample being modeled. As a result, the actual number of neighbors for such atoms will be smaller than under periodic boundary conditions.

So instead of first averaging the histogram bins to obtain the average atom counts  $\bar{n}_{ab}(r)$ , an individual local number density has to be calculated from any local histogram bin using the respective volume element for each central atom. Only then may the individual local number densities be averaged out to obtain the average number density. From it the rdf can be calculated using equation (3).

Whether a correction for the volume element is necessary depends on the position of the central atom and the size of the histogram bin (figure 1). In particular, the larger the volume element, the more likely it will protrude from the model spherical shell/surface, as shown in figure 1(a). On the left side of figure 1(a) the central atom is positioned inside the blue ring closer to the center of the sample and on the right side very close to the surface of the sample. The upper part of these figures shows histogram bins with a smaller radius  $r_1$ , while the lower part shows a larger histogram bin with radius  $r_2$ . For the same central atom position the volume element of the histogram bin is inside the sample for the smaller,  $r_1$  histogram bin (upper left part of figure), while protruding from the sample (shown in red) for the larger histogram bin with radius  $r_2$  (lower left part of figure 1(a)). The right side of the figure is showing histogram bins with different origin protruding from the sample to a different extent.

When the volume elements of each central atom are calculated, it may happen that some of those elements are

complete spherical shells (see the concentric circles with outer radius  $r_1$  on the upper left part of figure 1(a)), while others—fractions of spherical shells (shown in green in figure 1(b)) are obtained subtracting the protruding volume elements (shown in red in figure 1(b)) from the whole spherical shell.

First we will calculate the protruding volume element that is shown in red in figure 1(b). The radius of the smaller and larger spheres C and B are related as  $r_{B,j} = r_{C,j} + \Delta r = (j + 1)\Delta r$ , where  $\Delta r$  is the size of the histogram bin. The calculation can be divided into two steps, first calculating the protruding part of sphere B from sphere A,  $V_{out,B}$  (shown in yellow in figure 2(a)) and then calculating the protruding part of sphere C from sphere A,  $V_{out,C}$  (shown in orange figure 2(b)).

Note, the protruding volume depends on the radii of both spheres B and C, and the positions of their origins. For the sake of simplicity the origins are positioned at the middle of each central histogram bin during the derivation leading to only two independent variables for  $V_{out,B}$ ,  $V_{out,C}$ .

The volume of the spherical cap cut off from sphere A is denoted by  $V_{A,yB}(j, k)$  in figure 2(a). It can be computed as follows:

$$V_{A,yB}(j, k) = \frac{\pi}{3} x_B^2 (3R_0 - x_B) \quad (4)$$

where  $x_B = m_B + z - r_{B,j}$  is the height of the cap. The volume of the spherical cap cut off from sphere B,  $V_{B,yB}(j, k)$  (see figure 2(b)) can be calculated in a similar manner, i.e.

$$V_{B,yB}(j, k) = \frac{\pi}{3} m_B^2 (3r_B - m_B). \quad (5)$$

As shown in figures 2(a) and (b),  $z = R_0 - (k + 0.5)\Delta r$ . To determine  $x_B$ , the following two equations using the rules of a right angle triangle can be written (6). Note, from these

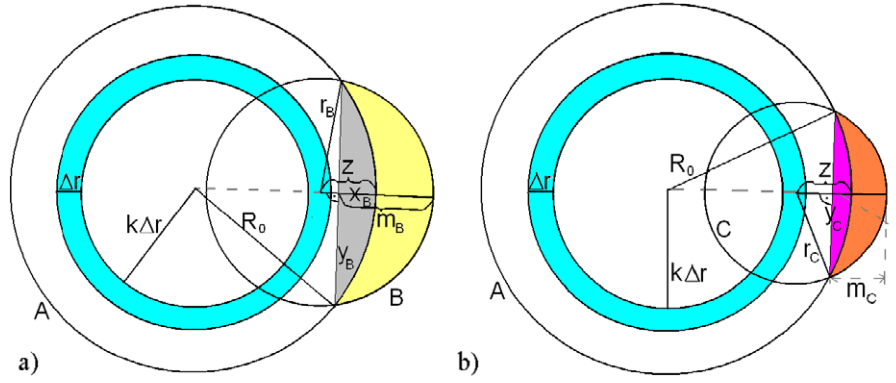


**Figure 2.** (a) Sketch of the volume elements of sphere B protruding from sphere A. The spherical caps of sphere A and B are cut off by the same plane and have a circular base with a radius of  $y_B$ . The volume of the spherical cap A (cut off from sphere A) is  $V_{A,yB}(j, k)$  (see (a), in gray), the volume of the spherical cap B cut off from sphere B is  $V_{B,yB}(j, k)$  (see the cumulated volume of gray and yellow in (a)). (b) The volume element of sphere C protruding from sphere A is shown. The spherical caps of sphere A and C cut off by the same plane have a circular base with  $y_C$  radius. The volume of the spherical cap A (cut off from sphere A) is  $V_{A,yC}(j, k)$  (see (a), pink) while the volume of the spherical cap C cut off from sphere C is  $V_{C,yC}(j, k)$  (shown in (b) in pink and orange).

equations both  $x_B$  and  $m_B$  can be determined.

$$\begin{aligned} \text{I. } R_0^2 &= (R_0 - x_B)^2 + y_B^2 \\ \text{II. } r_{B,j}^2 &= (z - x_B)^2 + y_B^2 \\ x_B &= \frac{z^2 - r_{B,j}^2}{2z - 2R_0}. \end{aligned} \quad (6)$$

As a result the volume designated in yellow in figure 2 can be calculated as follows:

$$V_{\text{out},B}(j, k) = V_{B,yB}(j, k) - V_{A,yB}(j, k). \quad (7)$$

Following the same reasoning scheme we can write that  $x_C = m_C + z - r_{C,j}$  where  $x_C$  and  $m_C$  are determined from equation (8).

$$\begin{aligned} \text{I. } R_0^2 &= (R_0 - x_C)^2 + y_C^2 \\ \text{II. } r_{C,j}^2 &= (z - x_C)^2 + y_C^2 \\ x_C &= \frac{z^2 - r_{C,j}^2}{2z - 2R_0}. \end{aligned} \quad (8)$$

The spherical caps with a circular base and a radius  $y_C$  cut off from spheres A and C can be calculated as follows:

$$\begin{aligned} V_{A,yC}(j, k) &= \frac{\pi}{3} x_C^2 (3R_0 - x_C) \\ V_{C,yC}(j, k) &= \frac{\pi}{3} m_C^2 (3r_C - m_C). \end{aligned} \quad (9)$$

The volume element of sphere C protruding from sphere A (shown in orange in figure 2(b)) is defined as  $V_{\text{out},C}(j, k) = V_{C,yC}(j, k) - V_{A,yC}(j, k)$ . Based on this definition, the protruding spherical shell (shown in red in figure 1(b)) can be computed as  $V_{\text{out}}(j, k) = V_{\text{out},B}(j, k) - V_{\text{out},C}(j, k)$ . Note all these relationships are valid when both spheres B and C are protruding from sphere A, which takes place if  $r_{B,j} - z > \Delta r$ . Given this, the volume element remaining inside sphere A is

$$\begin{aligned} V_{\text{in}}(j, k) &= \Delta V_j - V_{\text{out}}(j, k) \\ &= \frac{4}{3}\pi (r_{B,j}^3 - r_{C,j}^3) - V_{\text{out}}(j, k). \end{aligned} \quad (10)$$

If only sphere B is protruding from sphere A, which takes place if  $0 < r_{B,j} - z < \Delta r$ , the following relationship applies:  $V_{\text{out}}(j, k) = V_{\text{out},B}(j, k)$ , where  $V_{\text{in}}(j, k)$  is calculated according equation (10). If neither of spheres B and C are protruding from sphere A no volume element correction is necessary.

For each atom, a central bin index,  $k$  (see figure 2(b)), is assigned indicating which bin the atom belongs to. These bin indices are calculated at the beginning of the RMC simulation, and then updated when an atom is moved to another bin. The volume element  $V_{\text{in}}(j, k)$  will be the same for all the atoms belonging to the same central bin (with their distance,  $d$  from the origin between  $k\Delta r$  and  $(k+1)\Delta r$ ), as this is computationally more efficient than calculating and storing a series of individual volume elements for each atom. When  $\Delta r$  is small enough, this approximation will have little impact on the simulation results. Finally, in the case of non-periodic boundary conditions the average local density can be equation (11):

$$\bar{\rho}_{ab}(r) = \frac{1}{N_a} \sum_{m=1}^{N_a} \frac{n_{ab}^m(r)}{\Delta V_{\text{in}}(j, k)} = \frac{1}{N_a} \rho_{ab}^m(r)$$

$$j\Delta r \leq r < (j+1)\Delta r \quad k\Delta r \leq d_m < (k+1)\Delta r. \quad (11)$$

It is worth noting that while the system modeled is spherical in shape, its surface need not be smooth but may have edges and steps as it frequently occurs with real NPs. During the simulation atoms inside the spherical sample are moved around, and only those moves that keep the atoms within the model sphere are considered for acceptance according to the usual RMC acceptance scheme [12].

In figure 3 the correctly normalized rdf for a finite size, non-periodic, randomly distributed spherical model system is compared to an rdf of the same spherical sample situated in a cubic simulation box subject to periodic boundary conditions. The latter rdf shows unphysical sloping across the whole range of  $r$  values while the  $g(r)$  computed via equations (3) and (11) oscillates about one as it should according to its definition.

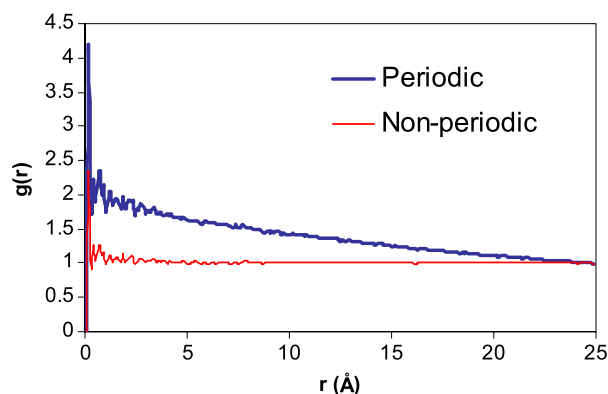


**Figure 3.** Behavior of the rdfs for a spherical randomly distributed sample calculated under periodic (blue) and non-periodic (red) boundary conditions. Note the unphysical sloping of the rdf computed under periodic boundary conditions.

## 2.2. Average coordination constraints

The calculation of the average coordination constraint under non-periodic boundary conditions has to be modified as well, in particular for atoms close to the surface of the spherical sample being modeled. Note those atoms will, on average, have a smaller number of neighbors than atoms in the sample's interior. Accordingly, the average coordination number is calculated only for atoms which are inside a sphere of radius  $R_0 - d$ , where  $d = (d_{\max} - d_{\min})/2$  and  $d_{\min}, d_{\max}$  are the limiting range values of the atomic coordination sphere.

## 3. Experimental and simulation details

### 3.1. Preparation of Ru nanoparticles

Polyvinylpyrrolidone (PVP,  $M_n = 10\,000$  g mol<sup>-1</sup>, Sigma Aldrich) stabilized Ru nanoparticles with a diameter of  $\sim 56$  Å were synthesized as part of a series of particles with different sizes [38] by using 1,4-butanediol or H<sub>2</sub> as the reducing agent. In a typical synthesis PVP/Ru molar ratio of 20 was applied. 30 mg of ruthenium(III) acetylacetonate (Aldrich) and 0.17 g of PVP were dissolved in 2 cm<sup>3</sup> of tetrahydrofuran (THF, Sigma Aldrich) and 3 cm<sup>3</sup> of 1,4-butanediol (Sigma Aldrich). This mixture was added to 27 cm<sup>3</sup> of 1,4-butanediol, which was preheated at 225 °C, followed by refluxing in a N<sub>2</sub> atmosphere for 2 h. The resulting black mixture was thoroughly washed with acetone and diethyl ether. After collecting the Ru nanoparticles by centrifugation, they were redispersed in 1.5 cm<sup>3</sup> distilled water. In cases where reduction was carried out in hydrogen, first 40 mg of RuCl<sub>3</sub>·xH<sub>2</sub>O (Alfa Aesar) and 0.22 g of PVP were dissolved in 1 cm<sup>3</sup> of distilled water in a 10 cm<sup>3</sup> autoclave. The autoclave was then pressurized with 20 bar H<sub>2</sub> followed by heating to 150 °C for 2 h under vigorous stirring. The resultant black mixture was washed, collected by centrifugation, and redispersed in 3 cm<sup>3</sup> distilled water.

### 3.2. TEM characterization

Transmission electron microscopy (TEM) was performed on a FEI Tecnai 20 electron microscope at an acceleration voltage of 200 kV with a LaB<sub>6</sub> filament. A small amount of the sample was diluted with ethanol, dispersed and dried over a carbon-coated Cu grid. Particle size distribution was calculated by measuring more than 150 particles. The NPs we studied had an average diameter of 56(±5) Å.

### 3.3. X-ray diffraction experiments

XRD data was collected at the beamline 11-ID-C at the Advanced Photon Source, Argonne National Laboratory, using x-rays of wavelength 0.1078 Å. The sample was in a glass capillary. An image plate detector was used. The XRD data were corrected for background and Compton scattering, normalized into absolute electron units using the RAD software [39].

Note that the high-energy XRD pattern and its Fourier counterpart, the atomic rdf, reflect assembly averaged structural features of all Ru nanoparticles sampled by the x-ray beam in the same way that traditional powder XRD represents an assembly average of all polycrystallites sampled by the x-ray beam in those experiments. Comparing a particle's assembly averaged structure features to a particle's assembly averaged properties (e.g., catalytic) puts the structure–property relationship exploration on the same footing.

### 3.4. RMC simulations

The RMC simulation was performed on a 6841 Ru atoms-containing spherical configuration closely resembling a spherical NP approximately 56 Å in diameter. The number density of 0.07439 Å<sup>-3</sup> corresponding to 12.45 g cm<sup>-3</sup> was used. A hexagonal closely packed (hcp) spherical configuration cut out from a crystalline lattice of Ru was used as a starting point of the RMC simulations. The simulations were guided by the experimental structure factor and were stopped when the RMC computed and experimental data agreed very well over the whole range of wavevectors reached by the present experiments, i.e. from about 2 to 30 Å<sup>-1</sup>. The simulation was carried out with the help of a new version of RMC\_POT software [31, 32] furnished for the case of non-periodic boundary conditions. Computations were done on an Intel® Xeon® CPU E5345 2.33 GHz 2\*quad core processor computer, using 4 threads. An average coordination constraint enforcing 12 first neighbors between 2.1 and 3.5 Å was applied to take into account the close-packed nature of the Ru metal structure.

## 4. Results and discussion

The RMC simulated and experimental XRD structure factors and their differences are shown in figure 4(a). The experimental structure factor shows broad diffraction features

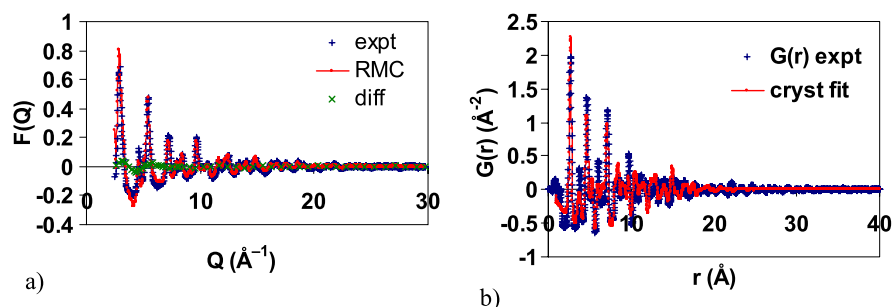


**Figure 4.** (a) The experimental (symbol +), the RMC-fitted (line) structure factors and their difference (symbol ×) of 28 Å radius Ru particles. (b) The ‘experimental’  $G(r)$  (symbol +) and the fit produced by the PDFgui program (line) assuming Ru hcp lattice periodicity.

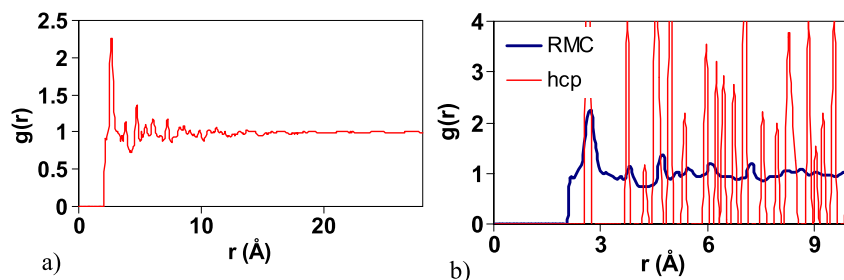


**Figure 5.** (a) The rdf for the RMC simulated model. (b) Low- $r$  parts of the rdfs for the RMC simulated model of Ru particles 28 Å in radius (line in blue) and for the crystalline hexagonal close packed (hcp) lattice of bulk Ru (line in red).

that are usually seen with heavily disordered materials. For comparison a fit to the ‘experimental’ PDF  $G(r)$  calculated by direct Fourier transformation of the experimental structure factor performed by the PDFgui [40] program assuming the lattice periodicity of bulk Ru hcp is shown in figure 4(b). The relationship between  $G(r)$  and  $g(r)$  is  $G(r) = 4\pi r \rho_0 (g(r) - 1)$ . As is visible, the major features are recreated, but there is a substantial difference in the peak heights showing that the periodic model cannot sufficiently reproduce the structure.

The simulated rdf  $g(r)$  is shown in figure 5(a). It decays to one at distances of about 15 Å, indicating that the Ru NPs studied by us exhibit only short to medium but definitely not long-range order.

The average coordination number in the interior of the NP model decreased a bit from 12 to 11.25 due to the presence of strong local disorder manifested by the broad character of the first rdf peak. The coordination numbers in the bulk are spreading from 7 to 17, 19% of the atoms having still 12 and 18% having 13 neighbors. The coordination numbers of the atoms at the NPs’ surface were considerably smaller than 12 due to free surface effects.

The rdfs of the hexagonal close packed lattice of bulk Ru and the RMC generated rdf for 28 Å radius Ru particles are compared in figure 5(b). As can be seen from the figure, the first rdf peak for the RMC generated model is considerably broadened when compared to the same peak in the rdf for bulk Ru. Note the first rdf peak for bulk Ru reflects the presence of 12 first atomic neighbors, 6 from the plane (denoted as A; see figure 6) where the atom chosen for the central one denoted as O resides, and 3–3 more (labeled as number 1, displayed in dark green) from the planes above and below this atom. This observation indicates that the first coordination sphere in

Ru NPs is considerably distorted when compared to the first coordination sphere of bulk Ru. The position of the second coordination sphere (containing six second neighbors labeled as number 2, light green in planes B) in Ru NPs has slightly moved to longer interatomic distances. Furthermore, the third rdf peak (coming from the atoms labeled as O’ in the next planes A above and below the atom in the origin) of the hcp lattice appears completely smeared out in the model rdf for Ru NPs. The fourth (planes B third neighbors, and same plane as origin second neighbors, neither shown in the picture) and fifth peaks (planes A above and below, atoms labeled as 1) of the hcp merged together for the NP, and further identification of the peaks is not possible.

A closer examination of the RMC generated configuration shown in figure 7 reveals that the hexagonally closed packed atomic planes of bulk Ru are still recognizable in the model for the 28 Å radius particles. This observation indicates that Ru NPs studied here share some of the structural features of their bulk counterpart. Next, we explored a 2.273 Å thick slice containing the central plane of the spherical sample cut out from the RMC generated model. Two different values for the spatial extent of the first atomic coordination sphere, 2.8 Å (figure 7(a)) and 3.5 Å (figure 7(b)), were used for the coordination number coloring. Note 2.8 Å is the radius of the first atomic coordination sphere in bulk Ru where each atom has 6 very first neighbors forming a flat planar atomic configuration (see figure 6). On the other hand, 3.5 Å is the first minimum in the RMC generated rdf which can be considered as a radius of the first coordination sphere for the Ru NPs under investigation. As can be seen in figure 7(a), only a few atoms have six first neighbors sitting on a flat plane. When 3.5 Å was applied as a cut off

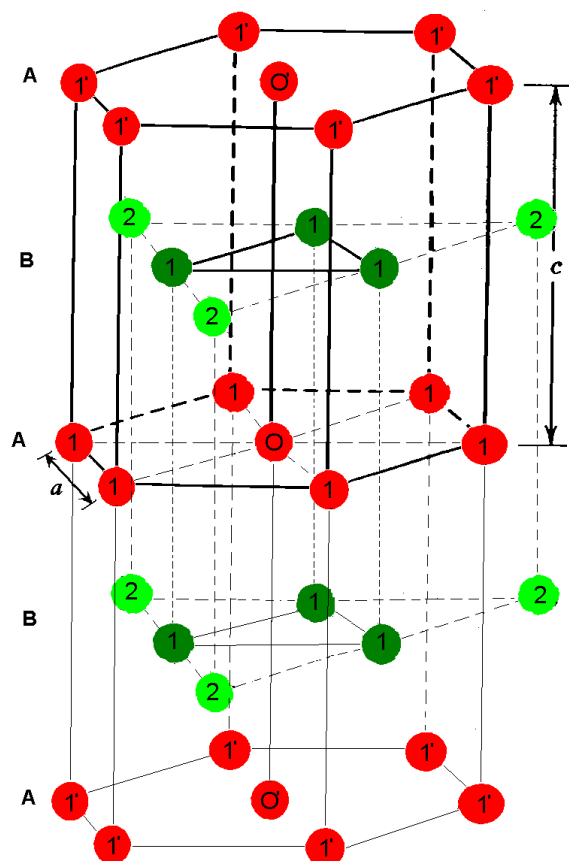


**Figure 6.** Two unit cells of the hcp structure of bulk Ru stacked on top of each other. The parameters of the hcp lattice are  $a = 2.7 \text{ \AA}$ ,  $c = 4.28 \text{ \AA}$ .

radius of the first coordination sphere, the number of atoms having 6 first neighbors forming a planar-type configuration increased considerably (see figure 7(b)). These results are

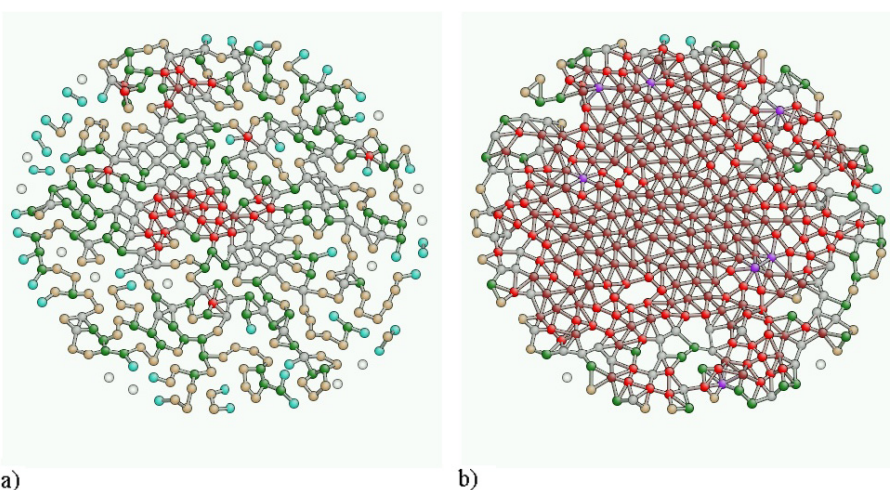


**Figure 7.** Slice containing the largest plane incorporating the  $a$ - $a$  crystallographic axis of the spherical RMC generated model for  $28 \text{ \AA}$  radius Ru particles. (a) A cut off value of  $2.8 \text{ \AA}$  was used for the upper limit of the atomic first coordination sphere. (b) A cut off value of  $3.5 \text{ \AA}$  was applied. The following coloring scheme was applied to differentiate between atoms with a different number of first atomic neighbors sitting on a plane: 0 neighbors: white; 1 neighbor: turquoise; 2 neighbors: beige; 3 neighbors: green; 4 neighbors: gray; 5 neighbors: red; 6 neighbors: brown; 7 neighbors: purple.

consistent with the substantial broadening of the first rdf peak indicating substantial disorder in the positions of the near atomic neighbors in Ru NPs.

To explore the three-dimensional structure of Ru NPs in more detail, a spherical cluster with a radius of  $5.1 \text{ \AA}$  was cut off from the very center of the RMC produced configuration, and displayed from two different points of view. The radius of  $5.1 \text{ \AA}$  was chosen since this real space distance entails the first five coordination spheres in bulk Ru. Again, a cut off distance of  $3.5 \text{ \AA}$  was applied as a radius of the first atomic coordination sphere. In figure 8(a) the cluster is presented along close packed atomic planes similar to the hcp planes occurring in bulk Ru. In figure 8(b) the same cluster is viewed from the direction of the  $c$  crystallographic axis, perpendicular to the planes. The results presented in figure 8(a) clearly show that (i) close packed though somewhat buckled atomic planes do exist in Ru NPs and (ii), as in bulk Ru, the planes are stacked up together. The atoms within these planes, however, are not arranged on the vertices of regular hexagons but are scattered in various in-plane directions (see figure 8(b)).

To check if the entire Ru NP model shares the features of its core discussed above, two orientational rdfs were computed in two orthogonal directions. One of the directions is along the  $c$  crystallographic axis in the Ru NP model, the other—perpendicular to that (labeled later as  $a$ - $a$ ). The orientational rdfs,  $g_c(r)$  and  $g_{a-a}(r)$  were calculated similarly to  $g(r)$  using appropriate normalizations due to the different sample volumes, and only those atom pairs were included in the calculation where the difference of the coordinate components of the atom pairs (in the case of  $g_c(r)$  perpendicular to the  $c$ -axis, in the case of  $g_{a-a}(r)$  perpendicular to the  $a$ - $a$  plane) were smaller than  $0.1 \text{ \AA}$ . The normalized auto-correlation function was calculated

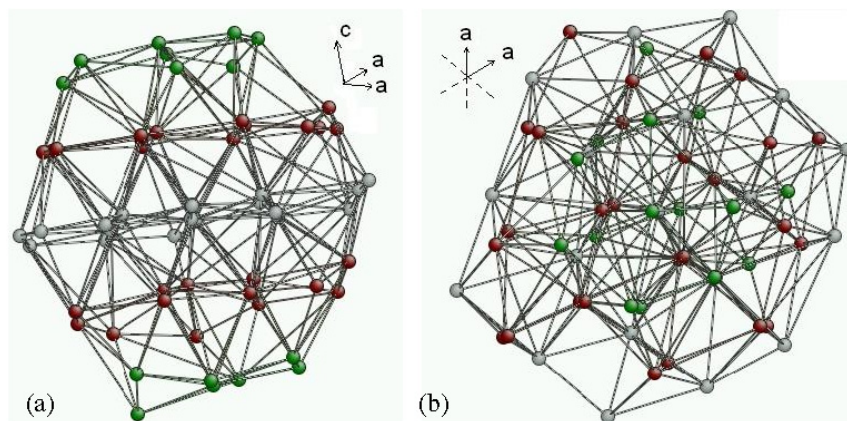


**Figure 8.** Spherical cluster with a radius of 5.1 Å cut out from the center of the RMC produced atomic configuration. The cluster is presented in two different orientations as described in the text. The coloring of the atoms reflects the atomic planes they belong to.

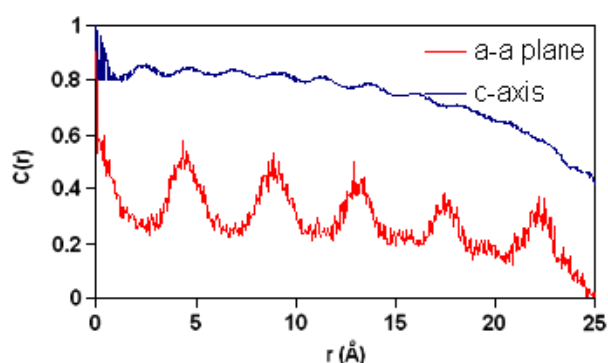


**Figure 9.** Auto-correlation functions for the orientational rdfs in Ru NPs calculated along the buckled atomic planes, (designated as *a*-*a* plane, line in red) and perpendicular to them (designated as *c* axis, line in blue).

according to the formula:

$$C(r_j) = \left( \frac{1}{N_j} \sum_i^{N_j} g(r_i)g(r_{i+j}) \right) / \left( \frac{1}{N_0} \sum_i^{N_0} g(r_i)g(r_{i+0}) \right) \quad (12)$$

where  $r_i, r_j$  are the  $i$ th and  $j$ th distance bin,  $N_j = N_{\max} - j$ . The auto-correlation functions of these rdfs are shown in figure 9. Results in the figure indicate much stronger interatomic correlations in a direction perpendicular to the atomic planes (along the *c*-axis). Correlation lengths were estimated from the asymptotic part of the auto-correlation functions,  $C(r)$ , using the relation:  $\ln(C(r)) \sim -(r/\xi)$ , where  $r$  is the radial distance and  $\xi$  is the so-called correlation length. The correlation lengths turned out to be about  $\xi_{a-a} = 18.9 \pm 0.1$  Å along the planes and  $\xi_c = 31.4 \pm 0.1$  in a direction perpendicular to the planes, clearly indicating that the degree of structural disorder in the studied RuNP of 28 Å radius is highly inhomogeneous.

## 5. Conclusion

A new method for reverse Monte Carlo-type simulations of the atomic-scale structure of spherical particles without

applying periodic boundary conditions was developed. When applied the method allows the testing and refining of structure models based directly on the diffraction data of spherical samples like nanoparticles with a free surface and, when present, inhomogeneities in the atomic ordering.

The method would perform best with diffraction data for particles with known size, a narrow size distribution and spherical shape. Note the method does not take into account possible inter-particle correlations. This is, however, not a severe limitation considering the fact that inter-particle correlations are typically long ranged. Such correlations are best revealed by small angle scattering, which is usually not included in the XRD data aimed at atomic rdf analysis.

The method was tested on Ru NPs approximately 28 Å in radius. Analysis of the resultant structure model showed that the NPs possess some of the structural features of bulk Ru, in particular the presence of close packed atomic layers that are stacked up together. The overall atomic-scale structure of the NPs, however, is quite distorted at both short and long-range atomic distance with the degree of structural disorder exhibiting a strong orientational dependence. This will definitely impact on the catalytic properties of the NPs which will be discussed elsewhere.

## Acknowledgment

The authors are thankful for financial support from DOE-BES via Grant DE-SC0006877.

## References

- [1] Yang S, Damiano M G, Zhang H, Tripathy S, Luthi A J, Rink J S, Ugolkov A V, Singh A T K, Dave S S, Gordon L I and Thaxton C S 2013 *Proc. Natl Acad. Sci.* **110** 2511
- [2] Jeong Y-H, Yoon H-J and Jang W-D 2012 *Polym. J.* **44** 512
- [3] Philip J, Kumar T J, Kalyanasundaram P and Raj B 2003 *Meas. Sci. Technol.* **14** 1289
- [4] Mornet S, Vasseur S, Grasset F, Verveka P, Goglio G, Demourgues A, Portier J, Pollert E and Duguet E 2006 *Prog. Solid State Chem.* **34** 237
- [5] Hyeon T 2003 *Chem. Commun.* 927

- [6] Elliott D W and Zhang W-X 2001 *Environ. Sci. Technol.* **35** 4922
- [7] Gupta A K and Gupta M 2005 *Biomaterials* **26** 3995
- [8] Lu A-H, Schmidt W, Matoussevitch N, Bönemann H, Spliethoff B, Tesche B, Bill E, Kiefer W and Schüth F 2004 *Angew. Chem. Int. Edn* **43** 4303
- [9] Petkov V, Bedford N, Knecht M R, Weir M G, Crooks R M, Tang W, Henkelman G and Frenkel A 2008 *J. Phys. Chem. C* **112** 8907–11
- [10] Petkov V, Moreels I, Hens Z and Ren Y 2010 *Phys. Rev. B* **81** 241304
- [11] Whitfield P and Mitchell L 2004 *Int. J. Nanosci.* **3** 757
- [12] McGreevy R L and Pusztai L 1988 *Mol. Simul.* **1** 359
- [13] McGreevy R L 1995 *Nucl. Instrum. Methods A* **354** 1
- [14] Gereben O and Pusztai L 1994 *Phys. Rev. B* **50** 14136  
Fukunaga T, Itoh K, Otomo T, Mori K, Sugiyama M, Kato H, Hasagawa M, Hirata A, Hirotsu Y and Aoki K 2006 *Physica B* **385** 259
- [15] Gereben O and Pusztai L 1994 *Mater. Sci. Eng.* **A179–A180** 433
- [16] Mile V, Gereben O, Kohara S and Pusztai L 2010 *J. Mol. Liq.* **157** 36
- [17] Billinge S J L and Levin I 2007 *Science* **316** 561
- [18] Rutledge R D, Morris H, Wellons M S, Zheng G, Shen J, Bentley J, Wittig J E and Lukehart M 2006 *J. Am. Chem. Soc.* **128** 14210
- [19] Sun S, Anders S, Thomson T, Baglin J E E, Toney M F, Hamann H F, Murray C B and Terris B D 2003 *J. Phys. Chem.* **107** 5419
- [20] van Aert S, Batenburg K J, Rossell M D, Erni R and van Tendeloo G 2011 *Nature* **470** 374
- [21] Egami T and Billinge S J L 2003 *Underneath the Bragg Peaks: Structural Analysis of Complex Materials* (Amsterdam: Elsevier)
- [22] Billinge S J L and Kanatzidis M G 2004 *Chem. Commun.* **2004** 749
- [23] Proffen Th and Billinge S J L 1999 *J. Appl. Crystallogr.* **32** 572
- [24] Toby B H, Egami T, Jorgensen J D and Subramanian M A 1990 *Phys. Rev. Lett.* **64** 2414
- [25] Tucker M G, Dove M T and Keen D A 2001 *J. Appl. Crystallogr.* **34** 630
- [26] Wells S A, Dove M T and Tucker M G 2002 *J. Phys.: Condens. Matter* **14** 4567
- [27] Sartbaeva A, Wells S A, Thorpe M F, Božin E S and Billinge S J L 2007 *Phys. Rev. Lett.* **99** 155503
- [28] Cervellino A, Giannini C and Guagliardi A 2006 *J. Comput. Chem.* **27** 995
- [29] Billinge S J L 2008 *J. Solid State Chem.* **181** 1695  
Proffen T 2006 *Rev. Mineral. Geochem.* **63** 255
- [30] Kodama K, Iikubo S, Taguchi T and Shamoto S 2006 *Acta Crystallogr. A* **62** 444–53
- [31] Gereben O and Pusztai L 2012 *J. Comput. Chem.* **33** 228
- [32] RMC.POT Website: [www.szfki.hu/~nphys/rmc++/opening.html](http://www.szfki.hu/~nphys/rmc++/opening.html)
- [33] Liu X, Yao K X, Meng C and Han Y 2012 *Dalton Trans.* **41** 1289–96
- [34] Rahman G, Yeon Lim J, Jung K-D and Joo O-S 2011 *Int. J. Electrochem. Sci.* **6** 2789–97
- [35] Zhao Y, Zhang J, Song J, Li J, Liu J, Wu T, Zhang P and Han B 2011 *Green Chem.* **13** 2078–82
- [36] Bedford N, Dablemont C, Viau G, Chupas P and Petkov V 2007 *J. Phys. Chem. C* **111** 18214
- [37] Lu F, Liu J and Xu J 2008 *Mater. Chem. Phys.* **108** 369–74
- [38] Hensen E J M 2012 unpublished
- [39] Petkov V 1989 *J. Appl. Crystallogr.* **22** 387
- [40] Farrow C L, Juhas P, Liu J W, Bryndin D, Božin E S, Bloch J, Proffen Th and Billinge S J L 2007 *J. Phys.: Condens. Matter* **19** 335219